Research Square

Preprints are preliminary reports that have not undergone peer review.
They should not be considered conclusive, used to inform clinical practice,
or referenced by the media as validated information.

# Collagen Ⅰ-DDR1 signaling promotes hepatocellular carcinoma cell stemness via Hippo signaling repression

**Yi-xiao Xiong**
Tongji Hospital
**Xiao-chao Zhang**
Tongji Hospital
**Jing-han Zhu**
Tongji Hospital
**Yu-xin Zhang**
Tongji Hospital
**Yong-long Pan**
Tongji Hospital
**Yu Wu**
Tongji Hospital
**Jian-ping Zhao**
Tongji Hospital
**Jun-jie Liu**
Tongji Hospital
**Yuan-xiang Lu**
Tongji Hospital
**Hui-fang Liang**
Tongji Hospital
**Zhan-guo Zhang**
Tongji Hospital
**Wan-guang Zhang** ( wgzhang@tjh.tjmu.edu.cn )
Tongji Hospital

**Research Article**

**Keywords:** Hepatocellular carcinoma, Cancer cell stemness, Collagen Ⅰ, DDR1, CD44, YAP

**Posted Date:** June 14th, 2022

**DOI:** https://doi.org/10.21203/rs.3.rs-1734316/v1

**License:** This work is licensed under a Creative Commons Attribution 4.0 International License. Read Full License

# Abstract

**Background:** Cancer stem cells (CSCs) are a minority population of cancer cells with stemness and multiple differentiation potentials, leading to cancer progression and therapeutic resistance. However, the concrete mechanism of CSCs remains obscure. Collagen Ⅻ-DDR1 signaling can response to ECM which can be a physical barrier that protects CSCs from chemotherapy. We explore the clinical significance, biological function and molecular mechanism of collagen Ⅻ-DDR1 signaling in promoting cancer cell stemness.

**Methods:** Picro-Sirius red staining was performed to distinguish collagen types. We established DDR1 knock-down and overexpression in different HCC cell lines. sphere-forming assay, single-cell colony formation, CD133 positive stem-like-cell proportion, and chemoresistance was performed to assess cancer cell stemness *in vitro*. Cancer cells limiting dilution implantation assay was conducted to assess stemness *in vivo.* Stemness and Hippo signaling associated genes expression was determined by quantitative RT-PCR. Proteins interaction was investigated by mass spectrometry, co-immunoprecipitation, GST pull-down and confocal microscopy imaging. The mechanisms of collagen Ⅻ-DDR1 regulating Hippo signaling were performed by RNA sequencing, immunoprecipitation and immunoblotting. A radiomic predicting model was constructed based on T2 weighted image, the predictive performance was evaluated by receiver operating characteristic curve (ROC) analysis.

**Results:** In advanced HCC tissues, collagen Ⅻ was upregulated, which was consistent with the expression of its receptor DDR1, high collagen Ⅻ levels accompanied by high DDR1 expression are associated with a poor prognosis in patients with HCC. Collagen Ⅻ-induced DDR1 activation enhanced HCC cell stemness *in vitro* and *in vivo*. Mechanistically, DDR1 interacts with CD44, which acts as a co-receptor that amplifies collagen Ⅻ-induced DDR1 signaling, and collagen Ⅻ-DDR1 signaling antagonized Hippo signaling by facilitating the recruitment of PP2AA to MST1, leading to exaggerated YAP activation. The combined inhibition of DDR1 and YAP synergistically abrogated HCC cell stemness. A radiomic model based on T2 weighted image can noninvasively predict collagen Ⅻ expression.

**Conclusions:** Our findings reveal the mechanism of collagen Ⅻ-DDR1 signaling inhibiting Hippo signaling, highlight the role of CD44/DDR1/YAP axis in promoting cancer cell stemness, and the radiomic model have potential of non-invasive predicting collagen Ⅻ expression, suggesting that DDR1 and YAP may serve as novel prognostic biomarkers and therapeutic targets in HCC.


# Introduction

Hepatocellular carcinoma (HCC) is one of the most prevalent causes of cancer-related mortality worldwide [1]. High tumor recurrence and metastasis rates are the primary reasons for the high mortality rate associated with HCC [2]. Chronic hepatitis, fibrosis, and cirrhosis increase the risk of HCC. The intratumor of HCC is constantly accompanied by desmoplasia and cirrhosis [3, 4]. Inflammation and extracellular matrix (ECM) deposition are characteristics of cirrhosis and the tumor microenvironment (TME). ECM serves as a physical scaffold that binds cells and tissues together and is pivotally involved in biochemical and biophysical signal transduction. Matrix deposition and remodeling cause tumor stiffness. Increased stiffness activates biomechanical signaling pathways that promote proliferation, invasiveness, and metastasis of cancer cells [5]. Recent studies have demonstrated that the ECM, especially collagen, contributes to immune exclusion in tumors with collagen-rich stroma [6-8]. Collagens are the primary and essential components of the ECM, an integral

component mechanics, and are hot off the press in cancer microenvironment research [9]. Collagens resist tensile stress because they stiffen as they are stretched in response to store growth-induced anxiety. Intratumor stress significantly decreases after collagen digestion [10].

High matrix stiffness induces and enhances the stemness of HCC cells [11]. Cancer stem cells (CSCs) are a group of cancer cells with stemness properties that possess self-renewal and differentiation capacities, leading to tumor progression, therapy resistance, metastasis, and recurrence [12, 13]. Increased ECM stiffness can be a physical barrier that protects CSCs from chemotherapeutic agents and $CD8^+$ T cell killing [14]. Changes in biomechanical properties, such as intrinsic softness, may be unique markers of CSCs [15].

In addition to the effects of external mechanics, the maintenance effect of collagen on tumor stem cells remains unclear. Collagen regulates cell function through its corresponding receptor discoidin domain receptor 1 (DDR1) [16]. DDR1 belongs to the receptor tyrosine kinase (RTKs) family and is mainly expressed in epithelial cells and mammalian tissues. Its specific ligands are natural collagen I~Ⅳ [17]. Our previous study showed that DDR1 enhanced hepatocellular carcinoma metastasis by recruiting PSD4 to ARF6 [18] and promoted HCC proliferation through the mTORC1 signaling pathway [19]. However, the role and precise mechanism of DDR1 in maintaining hepatocellular carcinoma stemness remain unclear.

Numerous upstream signals direct YAP/TAZ activity, including mechanical forces, cell adhesion, cell polarity, tyrosine kinase receptors, and cellular metabolism [20, 21]. Upon Hippo signaling off, nuclear YAP/TAZ are translocated from the cytoplasm, combined with the TEA domain transcription factor family (TEAD 1-4 [22]) directing gene expression programs [23, 24]. Based on the YAP-on and YAP-off classifications, restraining YAP may be an attractive therapeutic strategy for HCC, defined as the YAP-on stage [25]. YAP/TAZ are essential for cancer cells to reprogram into cancer stem cells and induce tumor initiation, progression, and metastasis [26]. However, the mechanism by which Hippo signaling affects HCC stemness has not yet been elucidated.

As one of the upstream receptors, CD44 is a broadly distributed non-kinase transmembrane glycoprotein that belongs to the cell adhesion molecule (CAMs) family, and is involved in cell physiological and pathological processes [27, 28]. Recent studies aim at the new function that CD44 acted as a co-receptor that mediated multiple RTKs inducing intracellular signal transduction [29, 30]. As an RTK family member, we speculated that DDR1 may be modified by CD44.

A preoperative and non-invasive method for evaluating collagen content is vital for surgeons because of the role of collagen I in HCC. Radiomics is an emerging imaging technique that can extract high-throughput imaging features from medical images and is frequently applied to predict the biological behavior of various tumors[31, 32]. Using radiomics signatures, we constructed a model for predicting collagen I expression in HCC.

This study showed that DDR1 stimulated by collagen I inhibited the Hippo pathway in HCC cells to maintain stemness through YAP nuclear translocation. Specifically, collagen I-induced DDR1 stimulation was augmented by the co-receptor CD44. DDR1 recruits PP2AA for MST1/2 dephosphorylation upon collagen I stimulation, thereby activating YAP translocation. Therefore, we identified a direct association between collagen I -DDR1 signaling and Hippo-YAP signaling in promoting HCC cells stemness. Furthermore, our studies indicate that inhibiting DDR1 signaling combined with disrupting YAP function could be a novel treatment method for HCC. A radiomics model based on T2-weighted images (T2WI) can evaluate relative collagen I expression to predict the prognosis and guide clinical treatment.

# Methods And Material

### Human tissue specimens and immunohistochemical analysis

From February 1, 2014 to December 31, 2015, 123 human tissues were authorized by the Hepatic Surgery Center, Tongji Hospital, Huazhong University of Science and Technology (Wuhan, China). All the participants provided written informed consent. Patients who had received radiotherapy or chemotherapy before surgery were excluded. Survival time was calculated from the date of surgery to the date of death or last follow-up. Tumor staging was performed according to the Seventh edition of the Tumor-Node-Metastasis (TNM) Classification of the International Union Against Cancer [33]. HCC samples (n=123) were used to generate a tissue microarray (Shanghai Biochip Co., Ltd. Shanghai, China). The fundamental processes of the Immunohistochemistry assay have been previously mentioned [18]. The pathological types of paraffin-embedded slides were rechecked by HE staining before IHC analysis. A DAB substrate kit (Zsbio Commerce Store) was used according to the manufacturer's instructions. Scores for staining frequency (0 <10%, 1 = 10–25%, 2 = 26–50%, 3 = 51–75%, 4 = >75%) and intensity (0 = negative, 1 = weak, 2 = moderate, 3 = intense staining) were used. A DAB substrate kit (Zsbio Commerce Store) was used according to the manufacturer's instructions. The overall staining score (OSS) was calculated by multiplying the staining area percentage score by the intensity score. 0–6 were considered low, and 9–12 were considered high. The results were scored by two pathologists who were blinded to clinicopathological data. All procedures were approved by the Ethics Committee of Tongji Hospital and conducted according to the Declaration of Helsinki Principles. Written and informed consent was obtained from each patient.

### Cell culture

HLF, Hep3B, SK-Hep1, and HEK293T cells were cultured in high-glucose Dulbecco's modified Eagle's medium (DMEM, HyClone, Illinois, USA) supplemented with 10% fetal bovine serum (FBS, Gibco, New York, USA), 100 U/ml penicillin and 100 mg/ml streptomycin (HyClone, Illinois, USA) at 37 °C with 5% $CO_2$. Collagen1 treatment was administered at a final concentration of 20 μg/ml. All the cell lines were obtained from the Hepatic Surgery Center, Tongji Hospital, Huazhong University of Science and Technology, China. 293 T cells were purchased from the China Center for Type Culture Collection (Wuhan, China).

### Sphere Assay

To calculate sphere-forming efficiency, cells were single-cell sorted into 96-well plates coated with an ultra-low attachment surface (Corning). The cells were grown under anchoring-independent conditions in selective serum-free DMEM/F12 medium supplemented with 1X B27 supplement minus vitamin A (LifeTechnologies), human recombinant EGF (hEGF) (R&D System) (20 ng/mL), and bFGF (R&D system) (20 ng/mL). After seven days, the spheres formed were counted.

### Colony formation assay.

Cells were suspended and seeded at a density of 1000 cells per well. After three weeks of cultivation, the cells were fixed and stained with 10% formalin and 0.1% crystal violet. The relative number of colonies was counted.

### Flow cytometric analysis.

Cells were stained with a PE-conjugated CD133 (BD Biosciences) antibody in PBS with 2% FBS at 4 °C for 30-60 mins. Isotype-matched mouse immunoglobulins were used as the controls. The samples were analyzed using the CytoFLEX flow cytometer and CytExpert software (Beckman Coulter).

### Drug resistance and IC50

Cells in the logarithmic growth phase were uniformly inoculated into 96-well plates (1000/well) and different diluted drug concentrations were added to the medium. Six replicate wells were used for each concentration gradient assay. The cells were cultured in an incubator for 48 h. Subsequently, 10 μL of CCK-8 solution (Vazyme, Nanjing, China) and 90 μL of culture medium were added, followed by incubation in the dark at 37 °C for 1 h. Absorbance at 450 nm was detected using GraphPad Prism (Version 8, GraphPad Software, San Diego, CA).

### Small interfering RNA, plasmids and lentivirus

Transient small interfering RNA (siRNA) assays were described before [34]. Sequences of siRNA are listed in Supplementary Table S4. Synthesizing siRNA duplexes were produced and validated by Ribobio (Guangzhou, China). Human DDR1 (NM_001954.4) cDNA and pcDNA3.1, plasmids were gifts from the Hepatic Surgery Center, Tongji Hospital, Huazhong University of Science and Technology, China. pBABE-puro (plasmid #1764), gag/pol (plasmid #14887), pMD2.G(plasmid #12259), pLKO.1 - TRC cloning vector (plasmid #10878), and psPAX2 (plasmid #12260) were purchased from Addgene (Cambridge, MA, USA). To establish pBABE- FLAG- DDR1, human cDNA was cloned into the BamHI/EcoRI site of the pBABE-puro retroviral vector and identified via sequencing (TSINGKE, Wuhan, China). To construct pLKO.1-scramble, pLKO.1-shDDR1, and pLKO.1- shCD44 plasmid, the target double-stranded oligonucleotides (shRNA) sequences, and one non-targeting sequence (negative control, scramble) were annealed and cloned into the AgeI/EcoRI site of the pLKO.1 vector. The shRNA oligo-pair sequences are listed in Supplementary Table S4. Viral production, infection, and establishment of stable cell clones have been described previously [35]. The pcDNA3.1 plasmid inserted by FlAG- or HA-tagged DDR1 and its mutants, FlAG- or HA-tagged CD44, FlAG-tagged PP2AA were constructed according to the ClonExpress II One Step Cloning Kit and Mut Express II Fast Mutagenesis Kit V2 (Vazyme, Nanjing, China) protocol and were identified by sequencing (TSINGKE, Wuhan, China). The CD44-overexpressing lentivirus was purchased from DesignGene Biotechnology (Shanghai, China)

### Coomassie blue staining and mass spectrometry

293 T cells transiently transfected with FLAG-DDR1 or FLAG-vector were lysed in IP lysis buffer (25mM Tris-HCl (pH 7.4), 150mM NaCl, 1% NP-40, 1mM EDTA, 10% glycerol, and protease inhibitor cocktail), and IP assays were performed as described previously [18]. The eluted proteins were separated by SDS-PAGE followed by coomassie blue staining. There was a significant difference in the gel bands between the FLAG-DDR1 and FLAG-vector groups among the molecular weight 70kd-125kd regions. Mass spectrometry was performed and analyzed using the ptm-bio lab (PTM BIO, Hangzhou, China).

### Reverse transcription PCR and Real-time quantitative PCR

Total cell RNA was extracted using TRIzol (Invitrogen, Carlsbad, CA, USA). Reverse transcription was carried out using HiScript II Q Select RT SuperMix (+gDNA wiper) (Vazyme, Nanjing, China) according to the manufacturer's instructions. Real-time fluorescence quantitative PCR was performed using the ChamQ Universal SYBR qPCR Master Mix (Vazyme, Nanjing, China). Gene expression levels were normalized to those of glyceraldehyde-3-

phosphate dehydrogenase (GAPDH) in the same samples. Each sample was analyzed independently in triplicate. The primers used are listed in Supplementary Table S5.

### Immunoblotting, co-immunoprecipitation (co-IP)

Immunoblotting and co-immunoprecipitation assays were performed as previously described [18]. Briefly, cells were collected and lysed on ice using IP lysis buffer. Lysates were incubated with protein G agarose for 2 h and immunoprecipitated with indicated antibodies overnight at 4 °C. The lysates were incubated with protein G agarose beads for 1 h followed by 1wash using IP lysis buffer and three washes with washing buffer (300mM NaCl, 1.0mM EDTA, 25mM Tris-HCl, pH7.4, 1.0% NP-40). The beads were eluted with 2×SDS-PAGE loading buffer and subjected to immunoblotting.

### Glutathione S transferase (GST) pull-down

The human DDR1 gene encoding was subcloned into a pET-42b vector. Following transformation and amplification in BL21(DE3) *E. coli*, recombinant GST-DDR1 fusion proteins were purified by GST Purification MagBeads (Absin Bioscience, Shanghai, China). GST (5 μg) or GST-DDR1 (5 μg) was incubated with recombinant human His-CD44 protein (5 μg) (ABclonal Technology, Wuhan, China) in PBS at 4 °C for 4 h under constant mixing. The bound proteins were incubated and immunoprecipitated with GST antibody-protein A beads (Absin Bioscience, Shanghai, China). After washing away the unbound proteins three times, the bound proteins were analyzed by SDS-PAGE and immunoblotting.

### Immunofluorescence and Confocal microscopy imaging.

Immunofluorescence assays were performed as described previously [34]. Briefly, after the indicated treatments, cells were cultured on coverslips for 12 h, fixed in 4% paraformaldehyde for 15 min at room temperature, and permeabilized with 0.5% Triton X-100 for 10 min. After blocking, slides were incubated with primary antibody overnight at 4 °C in a humidified box. The slides were then washed thrice and incubated with secondary antibody for 4 h at room temperature in a humidified box. Finally, the cell nuclei were stained with 40, 60-diamidino-2-phenylindole (DAPI, Sigma-Aldrich) for 5 min. The resulting signals were visualized using a confocal laser scanning microscope (Olympus FV1000, Tokyo, Japan).

### Dual-Luciferase Reporter Assay

Cells were seeded in a 24-well plate at a density of 10000 cells per well. The next day, cells were co-transfected with 200ng pGL4.17 and 4ng pRL-TK plasmids, and transfections were performed using Lipofectamine 3000 (Thermo Fisher Scientific, Waltham, MA, United States) according to the manufacturer's instructions. 12 h after transfection, cells were replaced with fresh medium and allowed to grow for 48 h. Luciferase activity was detected with the Dual-Luciferase Reporter Assay System (Promega, Madison, WI, United States) using a GloMax 20/20 Luminometer (Promega, Madison, WI, United States). Firefly luciferase activity was normalized to the Renilla luciferase activity.

### Reagents and antibodies

Rattail collagen I (BD Bioscience, MA, USA), Puromycin, trypsin-EDTA, Opti-MEM, and polybrene were obtained as previously described [19]. DDR1 inhibitor 7rh, and YAP inhibitor verteporfin were purchased from

MedChemExpress (Shanghai, China). The Lipofectamine 3000 reagent was purchased from Invitrogen (Life Technologies, Carlsbad, CA, USA). All the antibodies used in this study are listed in Supplementary Table S6.

### Extreme limiting dilution xenograft tumor formation

Thirty-six male NOD/SCID mice (4 weeks old) were divided into two groups (18 mice per group): a group receiving SK-Hep1 cells with vector and a group receiving cells overexpressing DDR1.The cells were diluted and transplanted by subcutaneous injection. Tumors were harvested at the end of the experiment for documentation. Tumor-initiating cell frequency was calculated using the extreme limiting dilution analysis (ELDA) software [36]. Animal assays were carried out according to Wuhan Medical Experimental Animal Care Guidelines.

### Drug treatments *in vivo*

Cells ($2 \times 10^6$) were subcutaneously injected into 4-week-old nude mice. After 2 weeks, the animals were orally administered verteporfin (50 mg/kg) and 7rh (50 mg/kg) twice daily for two weeks. Drugs delivered by oral gavage were dissolved in DMSO and diluted in corn oil. Control mice were treated with the vehicle following an identical procedure. Mice were killed (within 48 h of the last treatment), and samples were obtained for histopathological and immunohistochemical analysis.

### RNA-Seq

Cells were lysed using TRIzol reagent (Invitrogen, Life Technologies, Carlsbad, CA, USA). RNA extraction, library construction, high-throughput sequencing, and data analysis were conducted by Novogene Technology Co., Ltd. (Beijing, China).

### Tumor segmentation and feature extraction

65 patients were retrospectively recruited between February 1, 2014 and December 31, 2015. We randomly selected 45 cases as the training data set (25/20=positive/negative) and another 20 cases as the independent testing data set (11/9=positive/negative). Two independent readers manually delineated all MR images as high-resolution T2-weighted images (T2WI) using an open-source software package (ITK-SNAP, version 3.6.0, www.itksnap.org). Tumors were outlined as regions of interest (ROIs). Two types of images, “original images” and “wavelet images,” were used for the analysis in this study. “Original images” were the images without any transformation, and “wavelet images” were used for image denoising and improving image quality. The original images underwent a three-dimensional (i.e., x, y, and z directions) wavelet transformation using the PyWavelet package in Python. Each image was filtered by a high bandpass filter or low band-pass in the three directions, resulting in 8 combinations of different decompositions: LLH, LHL, HLL, LHH, HHL, HLH, HHH, and LLL (H means high, and L means low). The FeAture Explorer Pro (FAE Pro, V 0.4.1) was used to extract radiomic features. The shape features were extracted only from the “original images.” 18 types of first-order statistical features, 14 types of shape features, and 75 types of texture features [24 Gray Level Co-occurrence Matrix (GLCM) + 14 Gray Level Dependence Matrix (GLDM) + 16 Gray Level Run Length Matrix (GLRLM) + 16 Gray Level Size Zone Matrix (GLSZM) + 5 Neighborhood Gray-tone-difference Matrix (NGTDM)], a total of 107 “original images” features were used for analysis in our study. “Wavelet images” contained 144 first-order statistical features [8 wavelet images × 18] and 600 texture features [8 wavelet images × 75]. All 851 characteristics were extracted from the visible primary tumors, recorded, and stored quantitatively (Supplementary Table S7).

### Predictive models establishment

To remove the imbalance in the training data set, we used the synthetic minority oversampling technique (SMOTE) to balance the positive/negative samples. Normalization was applied to the feature matrix. Each feature vector was subtracted from the mean value of the vector and divided by its length. Because the dimension of the feature space was high, we compared the similarity of each feature pair. If the PCC value of the feature pair was greater than 0.99, one of them was removed. After this process, the feature space dimension was reduced, and each feature was independent. Before building the model, we used analysis of variance (ANOVA) to select features. The F-value was calculated to evaluate the relationship between the features and labels. We sorted the features according to their corresponding F-values and assigned a specific number of features to build the model. We used a support vector machine (SVM) as the classifier. The kernel function can map the features into a higher dimension to search the hyper-plane to separate cases with different labels. To determine the hyper-parameter of the model (e.g., the number of features), we applied a cross-validation 5-fold on the training data set. The hyper-parameters were selected according to model performance on the validation data-set. The model performance was evaluated using receiver operating characteristic (ROC) curve analysis. The area under the ROC curve (AUC) was calculated for quantification. Acuracy, sensitivity, specificity, positive predictive value (PPV), and negative predictive value (NPV) were also calculated at a cutoff value that maximized the value of the Yorden index. We also estimated the 95% confidence interval using bootstrapping with 1000 samples. The above processes were implemented using the FeAture Explorer Pro (FAEPro, V 0.4.1) on Python (3.7.6).

### Statistical analysis

Statistical analyses were performed using GraphPad Prism (Version 8, GraphPad Software, San Diego, CA). The levels of statistical significance for comparing the two groups were evaluated using the non-parametric two-sided Mann–Whitney U-test. To compare several groups with a control group, one-way ANOVA followed by Dunnett's multiple comparison test was applied. Two-way ANOVA followed by Bonferroni post-test was applied to compare several groups with a control group over time. Statistical significance was set at $P < 0.05$. Survival curves were generated using the Kaplan–Meier procedure. Survival curves and hazard ratios were evaluated using log-rank tests.

## Results

### High collagen I and DDR1 level predicts poor prognosis in HCC patients.

To analyze the types of collagens in the intratumor of HCC, we performed Picro-Sirius red staining in HCC tissues. The results showed that collagen I occupied the highest proportion of type □~□ collagens (Fig.1A). To explore the clinical significance of collagen I in HCC, we tested collagen I expression in a tissue microarray including 123 HCC tissue samples with corresponding clinicopathological features from Tongji Hospital (Supplementary Table S1). Compared with well-differentiated HCC tissues, collagen I was mainly highly expressed in moderately differentiated HCC tissues and was highest in poorly differentiated tissues (Fig. 1B). Kaplan–Meier analysis demonstrated that patients with high collagen I expression in tumors had a lower overall survival rate and a higher recurrence rate than patients with low collagen I expression (Fig.1C). Tumor sphere-forming assays showed the ability of collagen I in promoting HCC cell stemness (Fig.1D). Among the collagen I-

specific receptors [37], silencing DDR1 significantly reduced the Hep3B and HLF cells stemness induced by collagen I (Supplementary S1A).

To examine the clinical significance of DDR1 in HCC, we analyzed the levels of DDR1 in the same tissue microarray and TCGA databases. The results showed that DDR1 positively correlated with collagen I (Fig.1E–F, Supplementary S1B). Based on collagen I and DDR1 expression, patients were sorted into three groups: $Col1^{+}DDR1^{+}$(n= 54), double-high expression of collagen I/DDR1; $Col1^{+}DDR1^{-}$or $Col1^{-}DDR1^{+}$ (n=33), single-high expression of collagen I or DDR1; $Col1^{-}DDR1^{-}$ (n=36), double-low expression of collagen I/DDR1. Compared to the other groups, the $Col1^{+}DDR1^{+}$ group showed the shortest overall survival time and disease-free survival time (Fig.1G). In addition, DDR1 expression was elevated in HCC tissues compared to those in the corresponding adjacent non-tumor tissues. DDR1 was highly expressed in advanced TNM stages, poor tumor differentiation, advanced BCLC stage, and cirrhosis (Supplementary S1C–E, Supplementary Table S2). Kaplan–Meier analysis demonstrated that patients with high DDR1 expression had a lower overall survival rate and a higher recurrence rate (Supplementary S1F). In summary, the relationship between collagen I and DDR1 in clinical samples suggested that the synergistic impact of collagen I and DDR1 yielded a poor clinical outcome in HCC patients and they might play an essential role in the occurrence and development of HCC.

**Collagen I-DDR1 signaling enhances characteristics of cancer stemness.**

To verify the effect of DDR1 on HCC cell stemness *in vitro*, we performed sphere-forming assays. We found that the protein level of DDR1 was strongly upregulated in HCC spheres (referred to as CSCs) compared to the corresponding cultured adherent cells (referred to as non-CSCs) (Fig. 2A). As crucial transcription factors and membrane proteins in maintaining the self-renewal potential of stem cells [38], overexpression of DDR1 promoted mRNA expression of SOX2, NANOG, and EPCAM. Collagen I stimulation further amplified this effect. However, overexpression of the DDR1 kinase-dead (DDR1-K618A) and collagen-binding-defective (DDR1-R105A) mutants did not achieve this effect. In contrast, DDR1 knock-down diminished the expression of the former mRNA (Supplementary S2A). From TCGA database, DDR1 expression was positively correlated with CD133, which was verified by IHC of the tissue microarray (Fig. 2B–C). Furthermore, DDR1 overexpression or collagen I stimulation induced prominent promotion of sphere formation efficiency, number of CD133 positive cells, single-cell colony formation, and drug resistance to sorafenib or doxorubicin. In contrast, overexpression of DDR1-K618A and DDR1-R105A mutants failed to show the same results. In comparison, DDR1 depletion significantly reduced these CSC-related biological effects (Fig. 2D–G, Supplementary S2B–E).

*In vivo*, We used a xenograft model to examine the role of DDR1 in HCC cells. The subcutaneous tumors formed by DDR1 knock-down sphere-formed cells were significantly smaller than those formed by scramble cells (Fig. 3A). IHC results showed that the protein levels of DDR1, Ki67, and CD133 were higher in scrambled tumors than in DDR1 knock-down tumors (Fig. 3B). To further examine the role of DDR1 in tumor tumorigenesis, we injected NOD/SCID mice subcutaneously, with or without up-regulated DDR1 cells to conduct a limiting dilution assay. DDR1 overexpression markedly strengthened the tumor-forming ability and increased stem cell frequency (Fig. 3C–E). Together, the aforementioned confirmed that DDR1 promotes cell stemness and tumorigenesis in HCC *in vitro* and *vivo*, depending on its kinase activity and collagen stimulation.

**Collagen-induced DDR1 activation is synergistically promoted by CD44.**

To investigate the molecular mechanism of DDR1 in hepatocellular carcinoma, we studied its interacting partners using a combined IP/MS approach. SK-Hep1 cells were transfected with FLAG-DDR1 or FLAG-vector, and immunoprecipitated using anti-FLAG antibody. We found that CD44 (a CSCs marker) was one of the potential interacting partners of DDR1 (Fig. 4A)[18]. Co-immunoprecipitation (Co-IP) and glutathione S-transferase (GST) pull-down assays were performed, and the results from endogenous and exogenous assays showed that DDR1 interacted and combined with CD44 (Fig. 4B–C). In addition, the spatial co-localization of exogenous DDR1 and CD44 in 293T cells was detected by immunofluorescence and laser confocal scanning. A similar finding was observed for endogenous DDR1 and CD44 in the HLF cells (Fig. 4D). At the mRNA and protein levels, regulation was not observed between CD44 and DDR1 in Q-PCR and western blot assays (Supplementary S3.A–D). Next, we performed a co-IP assay with or without collagen I activation and found that collagen I increased the interaction between DDR1 and CD44 (Fig. 4E). As CD44 can act as a co-receptor to mediate receptor internalization, activation, degradation, or regulation of receptor kinase activity [39-41], we speculated whether CD44 could regulate collagen I-induced DDR1 activation. Co-IP assays indicated that CD44 knock-down decreased tyrosine phosphorylation of DDR1 (Fig. 4F). Overexpression of CD44 promoted the phosphorylation of DDR1 induced by collagen I treatment in a time-dependent manner. Knock-down of DDR1 reduced this effect in the HLF cells (Fig. 4G). Our results suggest that CD44 promotes the collagen I-induced activation of DDR1 in HCC cells. Whether the function of CD44 in HCC depends on DDR1 or not, we knocked down DDR1 in CD44-overexpressing HLF cells and overexpressed DDR1 in CD44 knock-down Hep3B cells. DDR1 depletion partially diminished the HCC cells in sphere formation efficiency, single-cell colony formation, CD133 positive stem-like-cell proportion, and chemoresistance driven by CD44 overexpression. Overexpression of DDR1 partially enhanced CSCs characteristics that were reduced by CD44 depletion within collagen I (Fig. 5A–D). The volume and weight of subcutaneous tumors developed by CD44 overexpression cells were significantly greater than those generated by the vector or CD44/shDDR1 cells (Fig. 5E). In summary, the above evidence suggests that DDR1 is a crucial protein required for CD44-mediated HCC cell stemness signaling.

### DDR1 inactivates Hippo signaling by facilitating the recruitment of PP2AA to MST1/2

To identify the pathways responsible for the influence of DDR1 on HCC cell stemness, we performed RNA sequencing of DDR1 knock-down HCC cells and control cells. KEGG pathway analysis revealed that Hippo signaling was significantly altered by DDR1 loss (Fig. 6A, Supplementary Table S3). Based on TCGA database, DDR1 was positively associated with YAP, CTGF, BCL2, and AXL (Supplementary S4A–D). Hippo signaling is closely associated with tumor stemness, we examined the effects of DDR1 on the expression of genes downstream of YAP/TAZ (Hippo pathway core proteins). The results showed that the mRNA levels of CTGF, CYR61, BCL2, and AXL were upregulated after the overexpression of DDR1 in Hep3B cells. The presence of collagen I further enhances these effects. In contrast, DDR1 knock-down significantly reduced the expression of CTGF, CYR61, BCL2, and AXL (Fig. 6B). The dual-luciferase reporter system suggested that DDR1 enhanced the YAP/TEAD-responsive element activity within collagen I (Fig. 6C). Nuclei-cytoplasmic fractionation and immunofluorescence assay indicated that DDR1 overexpression promoted the translocation of YAP into the nucleus (Fig. 6D–E). Western blotting showed that collagen I-stimulated DDR1 phosphorylation reduced MST1 phosphorylation and enhanced YAP activation, whereas DDR1 knock-down showed the opposite effect (Fig. 6F). These results indicated that collagen I-DDR1 signaling induces YAP activation.

protein phosphatase 2 scaffold subunit A alpha (PP2AA; PPP2R1A) as a canonical upstream phosphatase could dephosphorylate MST1/2 and inactivate Hippo signaling [42]. We analyzed DDR1 interacting partners. PP2AA is

a potential interacting protein with of DDR1 (Fig. 4A). Recruiting assays demonstrated that DDR1 promoted the recruitment of PP2AA to MST1 in a collagen-dependent manner (Fig. 6G). PP2AA depletion attenuated collagen I-DDR1 signaling-induced MST1 and LAST1 dephosphorylation, leading to YAP activation (Fig. 6H). These results indicated that PP2AA is necessary for collagen I -DDR1 signaling induced YAP activation.

In clinical samples, we evaluated p-DDR1, CD44, and YAP protein levels in 39 tissue samples from patients with HCC undergoing surgery at our hospital. The results showed that p-DDR1, CD44, and YAP levels were positively correlated in HCC tissues (Fig. 6I). Based on the IHC staining of collagen I, the samples were separated into collagen I-positive (collagen I +) and collagen I-negative (collagen I -) expression groups. We then performed multicolor immunofluorescence (IF) analyses to analyze the co-localization of these three proteins (Fig. 6J). As described above, p-DDR1 and CD44 levels were strongly correlated with YAP expression during collagen I deposition.

### Combined inhibition of DDR1 and YAP induces synergistic effects in HCC cell stemness.

To verify whether DDR1 functions via YAP, we used *in vitro and in vivo* treatments with the DDR1 inhibitor (7rh) [43] and the YAP inhibitor (verteporfin; VP) [44]. 7rh is an ATP-competitive oral DDR1-specific small-molecule inhibitor[45]. Verteporfin (VP), an inhibitor of YAP/TAZ, was identified in a small library of FDA-approved compounds and has been reported to sterically hinder the interaction between YAP and TEAD [46]. Treatment with 7rh or VP alone reduced the number of cells with sphere formation efficiency, colony formation, and CD133+ cell proportion and reduced the volume and weight of xenografts, respectively. Combination treatment with 7rh and VP further attenuated these effects compared to single agents (Fig. 7A–D). IHC results showed that Ki67 and CD133 staining was more intense in scrambled tumors than in 7rh or VP treatment tumors. The combination group yielded the lowest Ki67 and CD133 expression in tumors (Fig. 7E), and the combined treatment showed a favorable effect on anti-tumor therapy.

### Clinical-radiomics predictive model

Among the patients in the tissue microarray, we acquired 92 T2WI images, and a total of 65 patients were finally included in this retrospective study. The prediction model depends on the collagen I IHC score. Patients were divided into high and low groups. Model performance was evaluated using receiver operating characteristic (ROC) curve analysis. The results showed that the model based on 14 features obtained the highest AUC for the validation data set (Fig. 8A). At this point. The AUC and prediction accuracy of the model were 0.717 and 0.700, respectively, for the testing data-set. The clinical statistics for diagnosis and selected features are shown (Fig. 8B).

## Discussion

Dysregulation of the matricellular components of the tumor microenvironment has been linked to the development of metastases in multiple cancer types. The ECM is a non-cellular three-dimensional macromolecular network composed of collagens, elastin, laminins, fibronectin, proteoglycans, and other glycoproteins [47]. The exact mechanism of ECM in tumors has not yet been elucidated. In the present study, we aimed to identify the crucial components—collagen and its receptor DDR1. We found that the phosphorylation of DDR1 by collagen contributes to the maintenance of HCC cell stemness. In an attempt to identify collagen Ⅰ-DDR1 crucial for regulating CSCs, we found collagen Ⅰ-DDR1 signaling antagonized Hippo signaling with the help

of CD44 amplification. The combination of DDR1 and YAP inhibition is a logical target for anti-cancer stem cell-directed therapies, and a radiomic predictive model for collagen  can distinguish between chemotherapeutic efficacy and predicted prognosis. In recurrent HCC, mRNA and protein levels of DDR1 are higher in recurrent HCC than those in non-recurrent HCC [48]. High DDR1 expression is associated with advanced tumor stages [49]. Similar to the observations in our study, patients with DDR1 high expression had worse OS and DFS rates with accompanying collagen  deposition.

As a well-accepted theoretical model, cancer stem cells give rise to chemoresistance, metastasis, and recurrence in tumors. The CSCs model has been verified in various solid tumors, including HCC [50]. Extracellular matrix (ECM) rigidity segregates CSCs from chemotherapeutic agents as a physical defender and plays a critical role in tumor progression, especially in cancer cell stemness [14]. ECM stiffness contributes to NANOG activation and cancer stemness [51].

Extensive studies have demonstrated that ECM and collagens can cross-talk with cancer cells, including cancer stem cells, to promote tumor progression [52, 53]. Rich collagens in airway smooth muscle cells contribute to tumor cell colonization in the lung (55) and participate in cancer stemness, progression, and treatment [4, 54–56]. The above studies revealed that collagens could act as ligands that cross-talk with collagen receptors in the surrounding tumor cells [57] and that DDR1-dependent collagen remodeling contributes to immune exclusion in breast cancer [8]. This evidence suggests that CSCs tend to be enriched in stiffer microenvironment which warrants further in-depth studies. Our study demonstrated that through the corresponding receptor - DDR1, exogenous collagen I enhanced HCC cell stemness. Higher collagen I expression was positively correlated with DDR1 expression in clinical samples with poor prognosis. We demonstrated that collagen I - DDR1 signaling contributes to the maintenance of HCC stemness and progression.

DDR1, an RTKs, is upregulated in multiple cancers [58, 59]. We demonstrated that DDR1 mediates regulatory mechanisms involved in the maintenance of HCC cell stemness. Functionally, DDR1 is dependent on collagen I stimulation and its kinase activity. It interacts with CD44, which amplifies collagen I-induced DDR1 phosphorylation signaling, CD44/DDR1/YAP signaling axis acts as an inducer of the stemness of HCC cells by DDR1 activation. The results have not determined other components of the ECM that enhance collagen -induced DDR1 activation, and the role of different types of collagens in HCC stemness deserves further study.

CD44 promotes migration, invasion, and tumor progression by interacting with various proteins. Nevertheless, the regulatory relationship between CD44 and Hippo signaling is not directly precise [60, 61]. Rho A, merlin, and PI3K/Akt have been implicated in CD44-Hippo signaling [62–64]. A previous study demonstrated that CD44 acts as a ligand-binding membrane protein and co-receptor that mediates ligand-receptor-induced intracellular signal transduction [39]. In this study, CD44 was found to function as a co-receptor of DDR1 by negotiating and magnifying collagen I-DDR1 phosphorylation. Our research revealed a new interaction and was complementary to the analysis of the relationship between CD44 and Hippo signaling pathway.

Hippo signaling is an evolutionarily conserved pathway consisting of a network of signals to modulate tissue growth and organ size, and dysregulation of Hippo signaling contributes to human cancer progression [44, 65, 66]. Recent study indicated that DDR1 can sense the increasing matrix stiffness through control YAP/TAZ activity [67]. Our results further confirmed that collagen I - DDR1 signaling maintained HCC cell stemness by inhibiting Hippo signaling. STRIPAK integrates upstream signals to regulate the activities of MST1/2 and MAP4Ks, leading to the initiation of Hippo signaling [42]. We found that DDR1 acts as an adaptor protein that recruits PP2AA to

MST1. Our study is the first discovered collagen I - DDR1 signaling suppress Hippo signaling in maintaining HCC cell stemness.

Moreover, the DDR1 inhibitor – 7rh unveiled a significant treatment effect on pancreatic ductal adenocarcinoma and KRAS-mutant lung adenocarcinoma [68–70]. Originally, verteporfin was in clinical use as a photosensitizer in photocoagulation therapy for macular degeneration, and now it shows potential anti-cancer and anti-antifibrotic treatment in clinical trials and basic experiments [71–74]. The combination of 7rh and VP therapy had synergistic effects on reducing HCC cell stemness. In addition, VP decreased CD44 levels, and this positive feedback loop may be inactivated by disrupting DDR1 phosphorylation. These findings provide a theoretical basis and present novel therapeutic targets for HCC progression.

Since collagen I content estimates matter in the prognosis of inhibitor treatment, we can rely on radiomics to provide a non-invasive evaluation method for collagen I expression and needle biopsy. Radiomics applied within clinical-decision support systems to improve diagnostic, prognostic, and predictive accuracy is gaining importance in cancer research [75]. In this retrospective study, we constructed and validated T2WI radiomic signatures for the preoperative prediction of collagen I expression status in HCC. The radiomic model could predict collagen I expression and confirm its predictive value, which could be used to stratify patients into groups based on collagen I levels to guide treatment. This approach might allow clinicians to select more personalized and effective treatment strategies, as it demands more imaging samples and practice in the future.

# Conclusions

In summary, our results illustrate that collagen I -DDR1 signaling magnified by CD44 acts as a tumor motivator to promote HCC cell stemness by recruiting PP2AA to activate YAP. In HCC tissues, increased collagen I and DDR1 expression predicts poor prognosis and thus can serve as promising biomarkers and novel therapeutic strategies for HCC.

# Abbreviations

DDR1, discoidin domain receptor 1; HCC, hepatocellular carcinoma; GGT, γ-Glutamyl transpeptidase; Q-PCR, quantitative real-time PCR; Co-IP, co-immunoprecipitation; GST, glutathione S-transferase; WB, western blot; IHC, immunohistochemistry; IF, immunofluorescence.; CTGF, connective tissue growth factor; CYR61, cysteine rich angiogenic inducer 61; BCL2, BCL2 apoptosis regulator; AXL, AXL receptor tyrosine kinase; PP2AA, protein phosphatase 2 scaffold subunit A alpha.

# Declarations

### Ethics approval and consent to participate

All procedures were approved by the Ethics Committee of Tongji Hospital and conducted according to the Declaration of Helsinki Principles. Written and informed consent was obtained from each patient.

### Consent for publication

All authors give consent for the publication of the manuscript in *Journal of Hematology and Oncology.*

### Data Access Statement

Research data supporting this publication are available from the StarBase website: https://starbase.sysu.edu.cn/index.php [76].

### Competing interest

The authors declare that they have no conflict of interest.


### Funding

This study was supported by the National Natural Science Foundation of China (No. 81874149 to Wanguang Zhang; No. 82103606 to Xiaochao Zhang).


### Authors' contributions

WGZ contributed to the conception. XCZ and WGZ contributed to the study design. HFL and ZGZ form the overarching research goals and aims. YXX and XCZ wrote the main manuscript text. YXX, JHZ, YXZ and YLP contributed to the acquisition, analysis, and interpretation of the data. WGZ supervised the research activity planning. JJL and YXL verified the results/experiments and other research outputs. WGZ support the finance of the project. YW and JPZ critically revised the manuscript. All authors read and approve the final manuscript.


### Acknowledgements

We thank all study subjects for their participation in this study.


## References


1. Villanueva A. Hepatocellular Carcinoma. NEW ENGL J MED 2019;380:1450-1462.
2. Batlle E, Clevers H. Cancer stem cells revisited. NAT MED 2017;23:1124-1134.
3. Zamor PJ, DeLemos AS, Russo MW. Viral hepatitis and hepatocellular carcinoma: etiology and management. Journal of Gastrointestinal Oncology 2017;8:229-242.
4. Ma H, Chang H, Bamodu OA, Yadav VK, Huang T, Wu ATH, Yeh C, Tsai S, Lee W. Collagen 1A1 (COL1A1) Is a Reliable Biomarker and Putative Therapeutic Target for Hepatocellular Carcinogenesis and Metastasis. CANCERS 2019;11:786.
5. Nia HT, Munn LL, Jain RK. Physical traits of cancer. Science (American Association for the Advancement of Science) 2020;370:546.
6. Peng DH, Rodriguez BL, Diao L, Chen L, Wang J, Byers LA, Wei Y, Chapman HA, Yamauchi M, Behrens C, Raso G, Soto LMS, Cuentes ERP, Wistuba II, Kurie JM, Gibbons DL. Collagen promotes anti-PD-1/PD-L1 resistance in cancer through LAIR1-dependent CD8+ T cell exhaustion. NAT COMMUN 2020;11:4520.
7. Kuczek DE, Larsen AMH, Thorseth M, Carretta M, Kalvisa A, Siersbæk MS, Simões AMC, Roslind A, Engelholm LH, Noessner E, Donia M, Svane IM, Straten PT, Grøntved L, Madsen DH. Collagen density regulates the activity of tumor-infiltrating T cells. J IMMUNOTHER CANCER 2019;7:68.
8. Sun X, Wu B, Chiang H, Deng H, Zhang X, Xiong W, Liu J, Rozeboom AM, Harris BT, Blommaert E, Gomez A, Garcia RE, Zhou Y, Mitra P, Prevost M, Zhang D, Banik D, Isaacs C, Berry D, Lai C, Chaldekas K, Latham PS,

Brantner CA, Popratiloff A, Jin VX, Zhang N, Hu Y, Pujana MA, Curiel TJ, An Z, Li R. Tumour DDR1 promotes collagen fibre alignment to instigate immune exclusion. NATURE 2021.

9. Nissen NI, Karsdal M, Willumsen N. Collagens and Cancer associated fibroblasts in the reactive stroma and its relation to Cancer biology. J EXP CLIN CANC RES 2019;38:115.
10. Stylianopoulos T, Martin JD, Chauhan VP, Jain SR, Diop-Frimpong B, Bardeesy N, Smith BL, Ferrone CR, Hornicek FJ, Boucher Y, Munn LL, Jain RK. Causes, consequences, and remedies for growth-induced solid stress in murine and human tumors. Proc Natl Acad Sci U S A 2012;109:15101-15108.
11. You Y, Zheng Q, Dong Y, Xie X, Wang Y, Wu S, Zhang L, Wang Y, Xue T, Wang Z, Chen R, Wang Y, Cui J, Ren Z. Matrix stiffness-mediated effects on stemness characteristics occurring in HCC cells. Oncotarget 2016;7:32221-32231.
12. Llovet JM, Zucman-Rossi J, Pikarsky E, Sangro B, Schwartz M, Sherman M, Gores G. Hepatocellular carcinoma. NAT REV DIS PRIMERS 2016;2:16018.
13. Clarke MF. Clinical and Therapeutic Implications of Cancer Stem Cells. N Engl J Med 2019;380:2237-2245.
14. Plaks V, Kong N, Werb Z. The Cancer Stem Cell Niche: How Essential Is the Niche in Regulating Stemness of Tumor Cells? CELL STEM CELL 2015;16:225-238.
15. Lv J, Liu Y, Cheng F, Li J, Zhou Y, Zhang T, Zhou N, Li C, Wang Z, Ma L, Liu M, Zhu Q, Liu X, Tang K, Ma J, Zhang H, Xie J, Fang Y, Zhang H, Wang N, Liu Y, Huang B. Cell softness regulates tumorigenicity and stemness of cancer cells. The EMBO journal 2021;40:e106123.
16. Itoh Y. Discoidin domain receptors: Microenvironment sensors that promote cellular migration and invasion. Cell Adh Migr 2018;12:378-385.
17. Agarwal G, Mihai C, Iscru DF. Interaction of Discoidin Domain Receptor 1 with Collagen type 1. J MOL BIOL 2007;367:443-455.
18. Zhang X, Hu Y, Pan Y, Xiong Y, Zhang Y, Han M, Dong K, Song J, Liang H, Ding Z, Zhang X, Zhu H, Liu Q, Lu X, Feng Y, Chen X, Zhang Z, Zhang B. DDR1 promotes hepatocellular carcinoma metastasis through recruiting PSD4 to ARF6. ONCOGENE 2022.
19. Pan Y, Han M, Zhang X, He Y, Yuan C, Xiong Y, Li X, Zeng C, Lu K, Zhu H, Lu X, Liu Q, Liang H, Liao Z, Ding Z, Zhang Z, Chen X, Zhang W, Zhang B. Discoidin domain receptor 1 promotes hepatocellular carcinoma progression through modulation of SLC1A5 and the mTORC1 signaling pathway. CELL ONCOL 2022;45:163-178.
20. Dey A, Varelas X, Guan K. Targeting the Hippo pathway in cancer, fibrosis, wound healing and regenerative medicine. Nature reviews. Drug discovery 2020.
21. Meng Z, Moroishi T, Guan K. Mechanisms of Hippo pathway regulation. GENE DEV 2016;30:1-17.
22. Lamar JM, Stern P, Liu H, Schindler JW, Jiang Z, Hynes RO. The Hippo pathway target, YAP, promotes metastasis through its TEAD-interaction domain. P NATL ACAD SCI USA 2012;109:E2441-E2450.
23. Passaniti A, Brusgard JL, Qiao Y, Sudol M, Finch-Edmondson M. Roles of RUNX in Hippo Pathway Signaling. Singapore: Springer Singapore; 2017. pp 435-448.
24. Pobbati AV, Hong W. A combat with the YAP/TAZ-TEAD oncoproteins for cancer therapy. THERANOSTICS 2020;10:3622-3635.
25. Pearson JD, Huang K, Pacal M, McCurdy SR, Lu S, Aubry A, Yu T, Wadosky KM, Zhang L, Wang T, Gregorieff A, Ahmad M, Dimaras H, Langille E, Cole SPC, Monnier PP, Lok BH, Tsao M, Akeno N, Schramek D,

Wikenheiser-Brokamp KA, Knudsen ES, Witkiewicz AK, Wrana JL, Goodrich DW, Bremner R. Binary pan-cancer classes with distinct vulnerabilities defined by pro- or anti-cancer YAP/TEAD activity. CANCER CELL 2021;39:1115-1134.

26. Zanconato F, Cordenonsi M, Piccolo S. YAP/TAZ at the Roots of Cancer. CANCER CELL 2016;29:783-803.
27. Zöller M. CD44: can a cancer-initiating cell profit from an abundantly expressed molecule? NAT REV CANCER 2011;11:254-267.
28. Morath I, Hartmann TN, Orian-Rousseau V. CD44: More than a mere stem cell marker. The International Journal of Biochemistry & Cell Biology 2016;81:166-173.
29. Zhang H, Brown RL, Wei Y, Zhao P, Liu S, Liu X, Deng Y, Hu X, Zhang J, Gao XD, Kang Y, Mercurio AM, Goel HL, Cheng C. CD44 splice isoform switching determines breast cancer stem cell state. GENE DEV 2019;33:166-179.
30. Dhar D, Antonucci L, Nakagawa H, Kim JY, Glitzner E, Caruso S, Shalapour S, Yang L, Valasek MA, Lee S, Minnich K, Seki E, Tuckermann J, Sibilia M, Zucman-Rossi J, Karin M. Liver Cancer Initiation Requires p53 Inhibition by CD44-Enhanced Growth Factor Signaling. CANCER CELL 2018;33:1061-1077.
31. Chen M, Cao J, Hu J, Topatana W, Li S, Juengpanich S, Lin J, Tong C, Shen J, Zhang B, Wu J, Pocha C, Kudo M, Amedei A, Trevisani F, Sung PS, Zaydfudim VM, Kanda T, Cai X. Clinical-Radiomic Analysis for Pretreatment Prediction of Objective Response to First Transarterial Chemoembolization in Hepatocellular Carcinoma. Liver Cancer 2021;10:38-51.
32. Xu X, Zhang HL, Liu QP, Sun SW, Zhang J, Zhu FP, Yang G, Yan X, Zhang YD, Liu XS. Radiomic analysis of contrast-enhanced CT predicts microvascular invasion and outcome in hepatocellular carcinoma. J HEPATOL 2019;70:1133-1144.
33. Zhou L, Rui JA, Ye DX, Wang SB, Chen SG, Qu Q. Edmondson-Steiner grading increases the predictive efficiency of TNM staging for long-term survival of patients with hepatocellular carcinoma after curative resection. WORLD J SURG 2008;32:1748-1756.
34. Wu Y, Ding Z, Jin G, Xiong Y, Yu B, Sun Y, Wang W, Liang H, Zhang B, Chen X. Autocrine transforming growth factor-β/activin A-Smad signaling induces hepatic progenitor cells undergoing partial epithelial-mesenchymal transition states. BIOCHIMIE 2018;148:87-98.
35. Wu Y, Wang W, Peng XM, He Y, Xiong YX, Liang HF, Chu L, Zhang BX, Ding ZY, Chen XP. Rapamycin Upregulates Connective Tissue Growth Factor Expression in Hepatic Progenitor Cells Through TGF-beta-Smad2 Dependent Signaling. FRONT PHARMACOL 2018;9:877.
36. Hu Y, Smyth GK. ELDA: extreme limiting dilution analysis for comparing depleted and enriched populations in stem cell and other assays.; 2009. pp 70-78.
37. Cox TR. The matrix in cancer. NAT REV CANCER 2021;21:217-238.
38. Nio K, Yamashita T, Kaneko S. The evolving concept of liver cancer stem cells. MOL CANCER 2017;16:4.
39. Ponta H, Sherman L, Herrlich PA. CD44: From adhesion molecules to signalling regulators. NAT REV MOL CELL BIO 2003;4:33-45.
40. Joosten SPJ, Spaargaren M, Clevers H, Pals ST. Hepatocyte growth factor/MET and CD44 in colorectal cancer: partners in tumorigenesis and therapy resistance. Biochimica et biophysica acta. Reviews on cancer 2020;1874:188437.

41. Wang W, Zhang H, Liu S, Kim CK, Xu Y, Hurley LA, Nishikawa R, Nagane M, Hu B, Stegh AH, Cheng S, Cheng C. Internalized CD44s splice isoform attenuates EGFR degradation by targeting Rab7A. Proceedings of the National Academy of Sciences 2017;114:8366-8371.
42. Chen R, Xie R, Meng Z, Ma S, Guan K. STRIPAK integrates upstream signals to initiate the Hippo kinase cascade. NAT CELL BIOL 2019;21:1565-1577.
43. Dai W, Liu S, Wang S, Zhao L, Yang X, Zhou J, Wang Y, Zhang J, Zhang P, Ding K, Li Y, Pan J. Activation of transmembrane receptor tyrosine kinase DDR1-STAT3 cascade by extracellular matrix remodeling promotes liver metastatic colonization in uveal melanoma. Signal Transduction and Targeted Therapy 2021;6:176.
44. Huang Z, Zhou JK, Wang K, Chen H, Qin S, Liu J, Luo M, Chen Y, Jiang J, Zhou L, Zhu L, He J, Li J, Pu W, Gong Y, Li J, Ye Q, Dong D, Hu H, Zhou Z, Dai L, Huang C, Wei X, Peng Y. PDLIM1 Inhibits Tumor Metastasis Through Activating Hippo Signaling in Hepatocellular Carcinoma. HEPATOLOGY 2020;71:1643-1659.
45. Gao M, Duan L, Luo J, Zhang L, Lu X, Zhang Y, Zhang Z, Tu Z, Xu Y, Ren X, Ding K. Discovery and Optimization of 3-(2-(Pyrazolo[1,5-a ]pyrimidin-6-yl)ethynyl)benzamides as Novel Selective and Orally Bioavailable Discoidin Domain Receptor 1 (DDR1) Inhibitors. J MED CHEM 2013;56:3281-3295.
46. Liu-Chittenden Y, Huang B, Shim JS, Chen Q, Lee S, Anders RA, Liu JO, Pan D. Genetic and pharmacological disruption of the TEAD-YAP complex suppresses the oncogenic activity of YAP. GENE DEV 2012;26:1300-1305.
47. Karamanos NK, Theocharis AD, Neill T, Iozzo RV. Matrix modeling and remodeling: A biological interplay regulating tissue homeostasis and diseases. Matrix biology : journal of the International Society for Matrix Biology 2019;75-76:1-11.
48. Jian Z, Sun J, Chen W, Jin H, Zheng J, Wu Y. Involvement of discoidin domain 1 receptor in recurrence of hepatocellular carcinoma by genome-wide analysis. MED ONCOL 2012;29:3077-3082.
49. Shen Q, Cicinnati VR, Zhang X, Iacob S, Weber F, Sotiropoulos GC, Radtke A, Lu M, Paul A, Gerken G, Beckebaum S. Role of microRNA-199a-5p and discoidin domain receptor 1 in human hepatocellular carcinoma invasion. MOL CANCER 2010;9:227.
50. Toh TB, Lim JJ, Hooi L, Rashid MBMA, Chow EK. Targeting Jak/Stat pathway as a therapeutic strategy against SP/CD44+ tumorigenic cells in Akt/β-catenin-driven hepatocellular carcinoma. J HEPATOL 2020;72:104-118.
51. Pankova D, Jiang Y, Chatzifrangkeskou M, Vendrell I, Buzzelli J, Ryan A, Brown C, O'Neill E. RASSF 1A controls tissue stiffness and cancer stem-like cells in lung adenocarcinoma. The EMBO Journal 2019;38:e100532.
52. Lu P, Weaver VM, Werb Z. The extracellular matrix: A dynamic niche in cancer progression. J CELL BIOL 2012;196:395-406.
53. Biondani G, Zeeberg K, Greco MR, Cannone S, Dando I, Dalla Pozza E, Mastrodonato M, Forciniti S, Casavola V, Palmieri M, Reshkin SJ, Cardone RA. Extracellular matrix composition modulatesPDAC parenchymal and stem cell plasticity and behavior through the secretome. The FEBS Journal 2018;285:2104-2124.
54. Ezzoukhry Z, Henriet E, Piquet L, Boyé K, Bioulac-Sage P, Balabaud C, Couchy G, Zucman-Rossi J, Moreau V, Saltel F. TGF-β1 promotes linear invadosome formation in hepatocellular carcinoma cells, through DDR1 up-regulation and collagen I cross-linking. EUR J CELL BIOL 2016;95:503-512.
55. Juin A, Di Martino J, Leitinger B, Henriet E, Gary AS, Paysan L, Bomo J, Baffet G, Gauthier-Rouviere C, Rosenbaum J, Moreau V, Saltel F. Discoidin domain receptor 1 controls linear invadosome formation via a

Cdc42-Tuba pathway. J CELL BIOL 2014;207:517-533.

56. Zhong C, Tao B, Tang F, Yang X, Peng T, You J, Xia K, Xia X, Chen L, Peng L. Remodeling cancer stemness by collagen/fibronectin via the AKT and CDC42 signaling pathway crosstalk in glioma. THERANOSTICS 2021;11:1991-2005.
57. Xu S, Xu H, Wang W, Li S, Li H, Li T, Zhang W, Yu X, Liu L. The role of collagen in cancer: from bench to bedside. J TRANSL MED 2019;17:309.
58. Heinzelmann-Schwarz VA, Gardiner-Garden M, Henshall SM, Scurry J, Scolyer RA, Davies MJ, Heinzelmann M, Kalish LH, Bali A, Kench JG, Edwards LS, Bergh PMV, Hacker NF, Sutherland RL, O Brien PM. Overexpression of the Cell Adhesion Molecules DDR1, Claudin 3, and Ep-CAM in Metaplastic Ovarian Epithelium and Ovarian Cancer. CLIN CANCER RES 2004;10:4427-4436.
59. Valencia K, Ormazábal C, Zandueta C, Luis-Ravelo D, Antón I, Pajares MJ, Agorreta J, Montuenga LM, Martínez-Canarias S, Leitinger B, Lecanda F. Inhibition of Collagen Receptor Discoidin Domain Receptor-1 (DDR1) Reduces Cell Survival, Homing, and Colonization in Lung Cancer Bone Metastasis. CLIN CANCER RES 2012;18:969-980.
60. Lai C, Lin C, Liao W, Hour T, Wang H, Chuu C. CD44 Promotes Migration and Invasion of Docetaxel-Resistant Prostate Cancer Cells Likely via Induction of Hippo-Yap Signaling. CELLS-BASEL 2019;8:295.
61. Orian-Rousseau V. CD44 Acts as a Signaling Platform Controlling Tumor Progression and Metastasis. FRONT IMMUNOL 2015;6:154.
62. Fan Z, Xia H, Xu H, Ma J, Zhou S, Hou W, Tang Q, Gong Q, Nie Y, Bi F. Standard CD44 modulates YAP1 through a positive feedback loop in hepatocellular carcinoma. BIOMED PHARMACOTHER 2018;103:147-156.
63. Li S, Li C, Zhang Y, He X, Chen X, Zeng X, Liu F, Chen Y, Chen J. Targeting Mechanics-Induced Fibroblast Activation through CD44-RhoA-YAP Pathway Ameliorates Crystalline Silica-Induced Silicosis. THERANOSTICS 2019;9:4993-5008.
64. Xu Y, Stamenkovic I, Yu Q. CD44 Attenuates Activation of the Hippo Signaling Pathway and Is a Prime Therapeutic Target for Glioblastoma. CANCER RES 2010;70:2455-2464.
65. Han Y. Analysis of the role of the Hippo pathway in cancer. J TRANSL MED 2019;17:116.
66. Zhang Z, Qiu N, Yin J, Zhang J, Liu H, Guo W, Liu M, Liu T, Chen D, Luo K, Li H, He Z, Liu J, Zheng G. SRGN crosstalks with YAP to maintain chemoresistance and stemness in breast cancer cells by modulating HDAC2 expression. THERANOSTICS 2020;10:4290-4307.
67. Ngai D, Mohabeer AL, Mao A, Lino M, Bendeck MP. Stiffness-Responsive Feedback Autoregulation of DDR1 Expression is Mediated by a DDR1-YAP/TAZ Axis. MATRIX BIOL 2022.
68. Ambrogio C, Gómez-López G, Falcone M, Vidal A, Nadal E, Crosetto N, Blasco RB, Fernández-Marcos PJ, Sánchez-Céspedes M, Ren X, Wang Z, Ding K, Hidalgo M, Serrano M, Villanueva A, Santamaría D, Barbacid M. Combined inhibition of DDR1 and Notch signaling is a therapeutic strategy for KRAS-driven lung adenocarcinoma. NAT MED 2016;22:270-277.
69. Nokin M, Darbo E, Travert C, Drogat B, Lacouture A, San José S, Cabrera N, Turcq B, Prouzet-Mauleon V, Falcone M, Villanueva A, Wang H, Herfs M, Mosteiro M, Jänne PA, Pujol J, Maraver A, Barbacid M, Nadal E, Santamaría D, Ambrogio C. Inhibition of DDR1 enhances in vivo chemosensitivity in KRAS-mutant lung adenocarcinoma. JCI Insight 2020;5.

70. Aguilera KY, Huang H, Du W, Hagopian MM, Wang Z, Hinz S, Hwang TH, Wang H, Fleming JB, Castrillon DH, Ren X, Ding K, Brekken RA. Inhibition of Discoidin Domain Receptor 1 Reduces Collagen-mediated Tumorigenicity in Pancreatic Ductal Adenocarcinoma. MOL CANCER THER 2017;16:2473-2485.
71. Huggett MT, Jermyn M, Gillams A, Illing R, Mosse S, Novelli M, Kent E, Bown SG, Hasan T, Pogue BW, Pereira SP. Phase I/II study of verteporfin photodynamic therapy in locally advanced pancreatic cancer. BRIT J CANCER 2014;110:1698-1704.
72. Zhao X, Wang X, Fang L, Lan C, Zheng X, Wang Y, Zhang Y, Han X, Liu S, Cheng K, Zhao Y, Shi J, Guo J, Hao J, Ren H, Nie G. A combinatorial strategy using YAP and pan-RAF inhibitors for treating KRAS-mutant pancreatic cancer. CANCER LETT 2017;402:61-70.
73. Garcia-Rendueles MER, Ricarte-Filho JC, Untch BR, Landa I, Knauf JA, Voza F, Smith VE, Ganly I, Taylor BS, Persaud Y, Oler G, Fang Y, Jhanwar SC, Viale A, Heguy A, Huberman KH, Giancotti F, Ghossein R, Fagin JA. NF2 Loss Promotes Oncogenic RAS-Induced Thyroid Cancers via YAP-Dependent Transactivation of RAS Proteins and Sensitizes Them to MEK Inhibition. CANCER DISCOV 2015;5:1178-1193.
74. Islam MS, Afrin S, Singh B, Jayes FL, Brennan JT, Borahay MA, Leppert PC, Segars JH. Extracellular matrix and Hippo signaling as therapeutic targets of antifibrotic compounds for uterine fibroids. Clinical and translational medicine 2021;11:e475.
75. Lambin P, Leijenaar RTH, Deist TM, Peerlings J, de Jong EEC, van Timmeren J, Sanduleanu S, Larue RTHM, Even AJG, Jochems A, van Wijk Y, Woodruff H, van Soest J, Lustberg T, Roelofs E, van Elmpt W, Dekker A, Mottaghy FM, Wildberger JE, Walsh S. Radiomics: the bridge between medical imaging and personalized medicine. Nature reviews. Clinical oncology 2017;14:749-762.
76. Li J, Liu S, Zhou H, Qu L, Yang J. starBase v2.0: decoding miRNA-ceRNA, miRNA-ncRNA and protein-RNA interaction networks from large-scale CLIP-Seq data. NUCLEIC ACIDS RES 2014;42:D92-D97.

# Figures

Figure 1

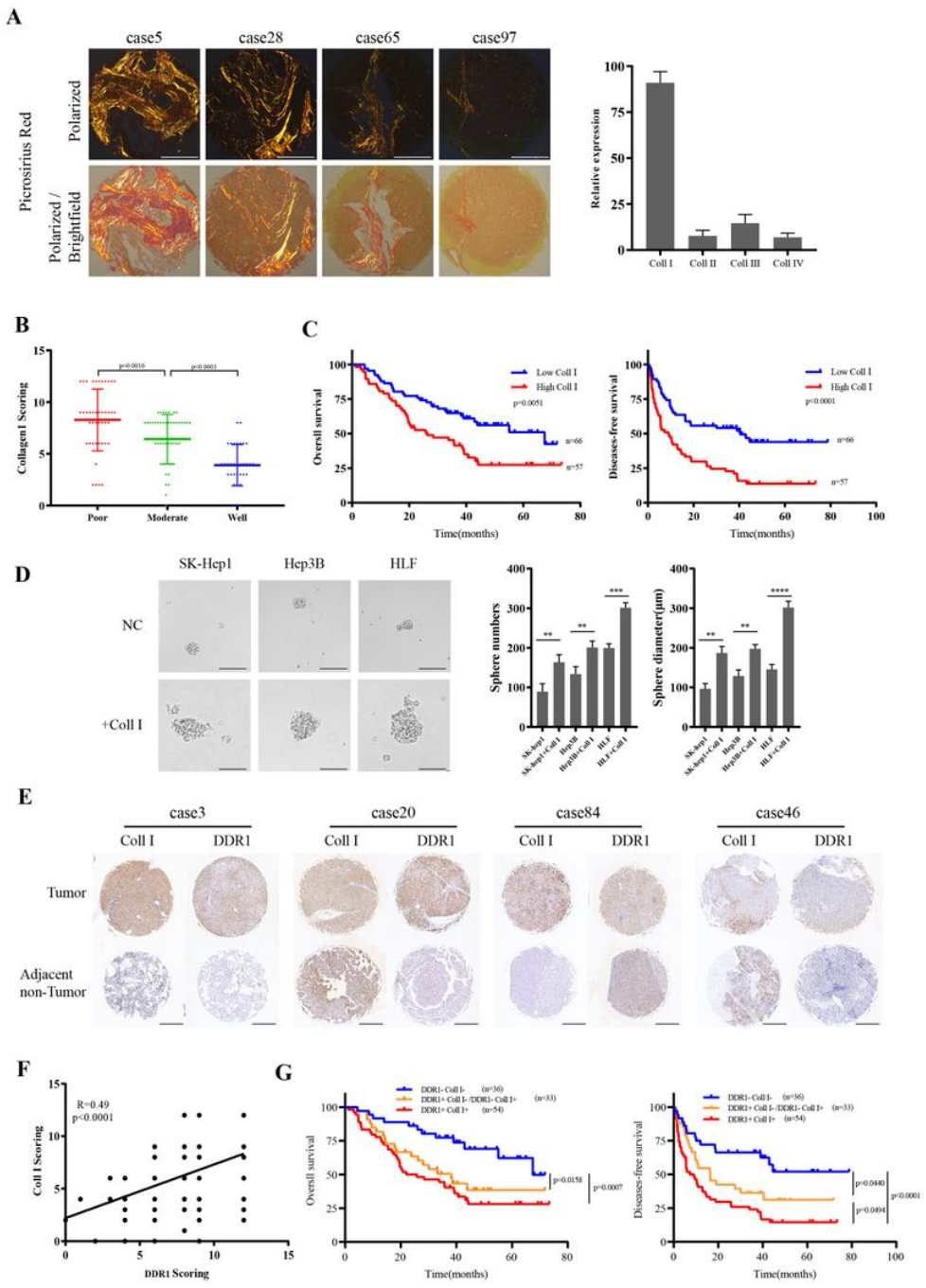


## Figure 1

### Clinical significance of Collagen Ⅰ and DDR1 in clinical patients with HCC

(A) Picrosirius red staining for collagen type in specimens of HCC patients (scale bar =500μm).

(B) Immunohistochemistry (IHC) staining analyses of collagen Ⅰ in specimens of HCC patients with tumor differentiation.

(C) Based on IHC staining, cohorts were divided into two groups: Collagen Ⅰ $^{high}$, n=57; Collagen Ⅰ $^{low}$, n=66. Kaplan-Meier's analysis of collagen Ⅰ expression level with the overall survival and disease-free survival rate in

HCC patients.

(D) Effects of SK-Hep1, Hep3B, or HLF with or without collagen Ⅰ stimulation on sphere-forming capacity, including sphere numbers and diameters (scale bar=200μm).

(E) Representative result of IHC staining for collagen Ⅰ and DDR1 in pair specimens of HCC patients (scale bar =500μm).

(F) Correlation of collagen Ⅰ and DDR1 IHC staining score.

(G) Kaplan-Meier's analysis of 3 groups of Collagen Ⅰ and DDR1 expression levels with the overall survival and disease-free survival rate in HCC patients. Redline: Collagen Ⅰ $^{high}$ DDR1 $^{high}$, n=54; Orange line: Collagen Ⅰ $^{low}$ DDR1 $^{high}$ or Collagen Ⅰ $^{high}$ DDR1 $^{low}$, n=33; Blue line: Collagen Ⅰ $^{low}$ DDR1 $^{low}$, n=36.

Pearson's test was used to calculate the correlation between protein expression levels. The log-rank test was used to calculate the differences between individual groups. Two-tailed unpaired Student's t-test was performed. Each bar represents the mean ± SD.*$p < 0.05$, **$p < 0.01$, and ***$p < 0.001$.

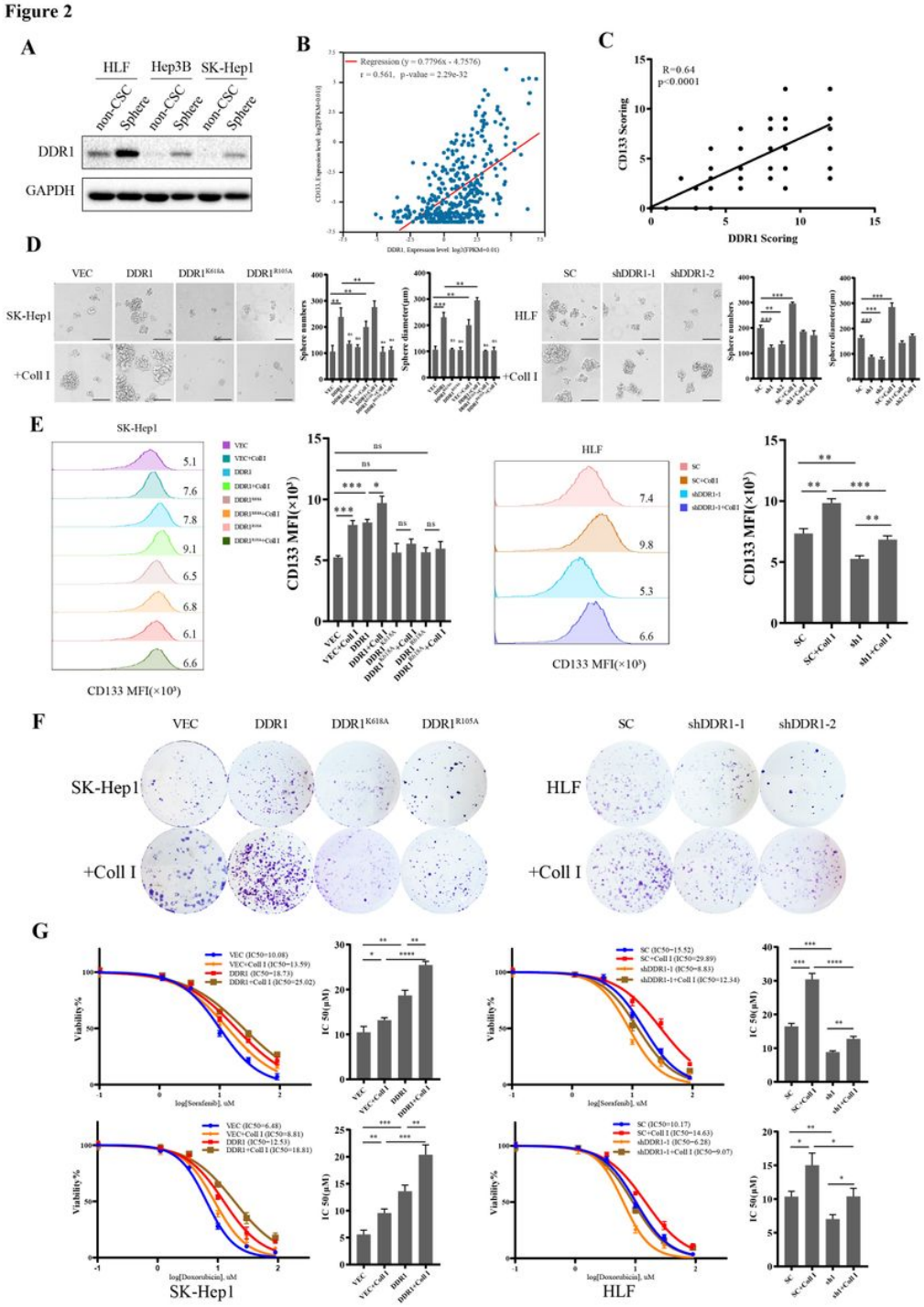


## Figure 2

**DDR1 enhances the stemness of HCC cell lines *in vitro*.**

(A) DDR1 expression in non-sphere and sphere-forming HCC cell lines. GAPDH was used as a loading control.

(B) The relationship between DDR1 and CD133 was evaluated in the TCGA cohort (n=374).

(C) Correlation of DDR1 and CD133 in IHC staining score.

(D) Effects of DDR1 knock-down or overexpress WT, mutant DDR1$^{K618A}$, and DDR1$^{R105A}$ HCC cell lines on sphere-forming capacity, including sphere numbers and diameters (scale bar=200μm).

(E) Flow cytometry analyses of the CD133 mean fluorescence intensity in DDR1 knock-down or overexpress WT, mutant DDR1$^{K618A}$, and DDR1$^{R105A}$ HCC cell lines. Error bars represent the standard deviation from three times independent experiments.

(F) Colony formation assay of the DDR1 knock-down or overexpress WT, mutant DDR1$^{K618A}$, and DDR1$^{R105A}$ HCC cell lines.

(G) DDR1 knock-down or overexpress HCC cell lines, drug resistance to sorafenib or doxorubicin. Cell viability was compared with the untreated cells, and IC50 values were calculated.

Pearson's test was used to calculate the correlation between protein expression levels. Two-tailed unpaired Student's t-test was performed. Each bar represents the mean ± SD.*$p < 0.05$, **$p < 0.01$, and ***$p < 0.001$.

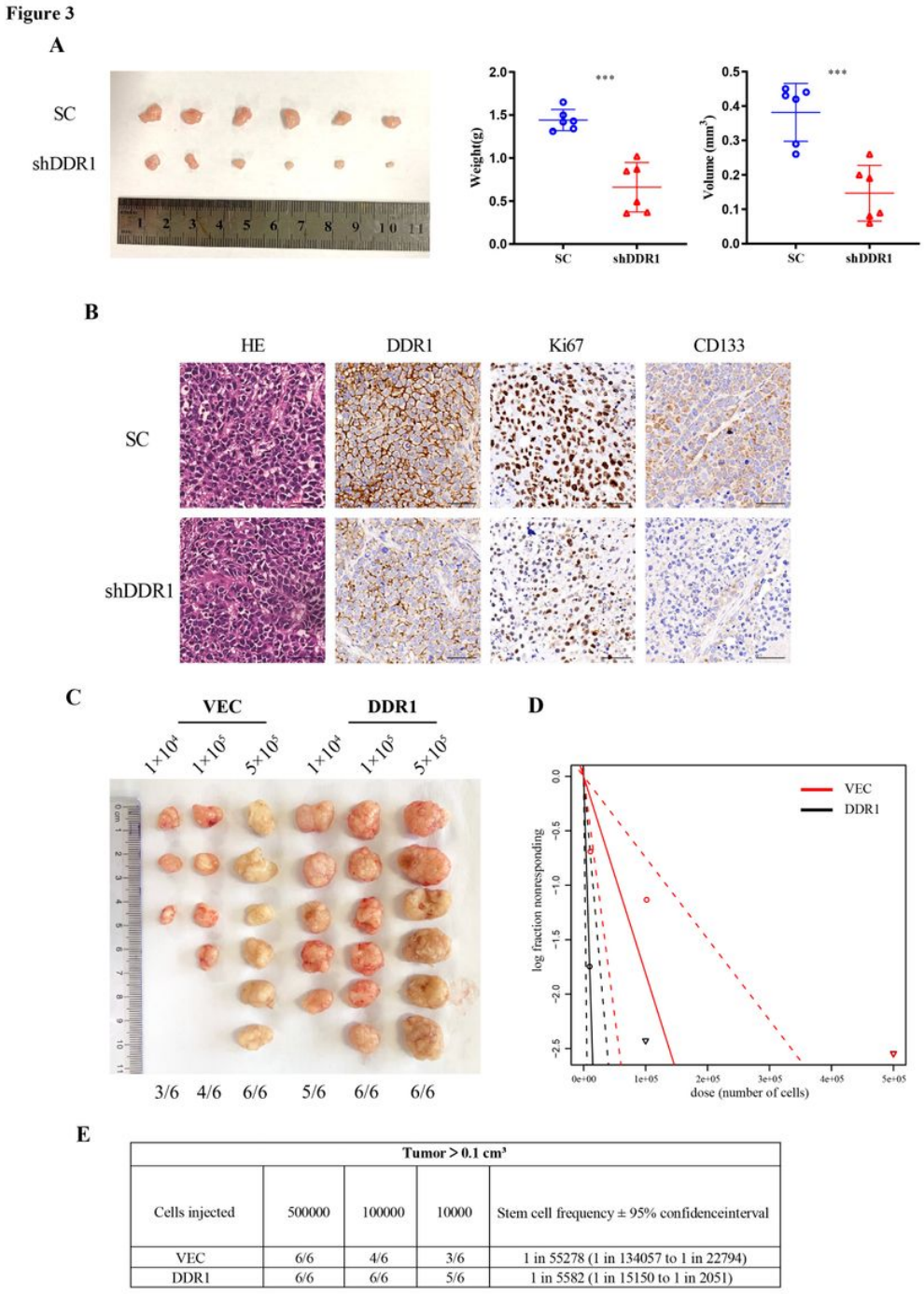


| Tumor > 0.1 cm³ | | | | |
|---|---|---|---|---|
| Cells injected | 500000 | 100000 | 10000 | Stem cell frequency ± 95% confidenceinterval |
| VEC | 6/6 | 4/6 | 3/6 | 1 in 55278 (1 in 134057 to 1 in 22794) |
| DDR1 | 6/6 | 6/6 | 5/6 | 1 in 5582 (1 in 15150 to 1 in 2051) |

## Figure 3

### DDR1 enhances the stemness of HCC cell lines *in vivo*.

(A) 4 -week-old male nude mice were subcutaneously injected by sphere-formed DDR1 knock-down HCC cell line (n=6/group). Tumor weight and volume were shown in the right panel.

(B) Representative images of IHC staining of HE, DDR1, Ki67, and CD133 (scale bar=100μm).

(C) Extreme limiting dilution analysis, DDR1 overexpressed HCC cells were serially diluted and then subcutaneously injected into 4 -week-old male NOD/SCID mice(n=6/group).

(D–E) Tumor formation ability and stem cell frequency were analyzed.

Two-tailed unpaired Student's t test was performed. Each bar represents the mean ± SD.*p < 0.05, **p < 0.01, and ***p < 0.001

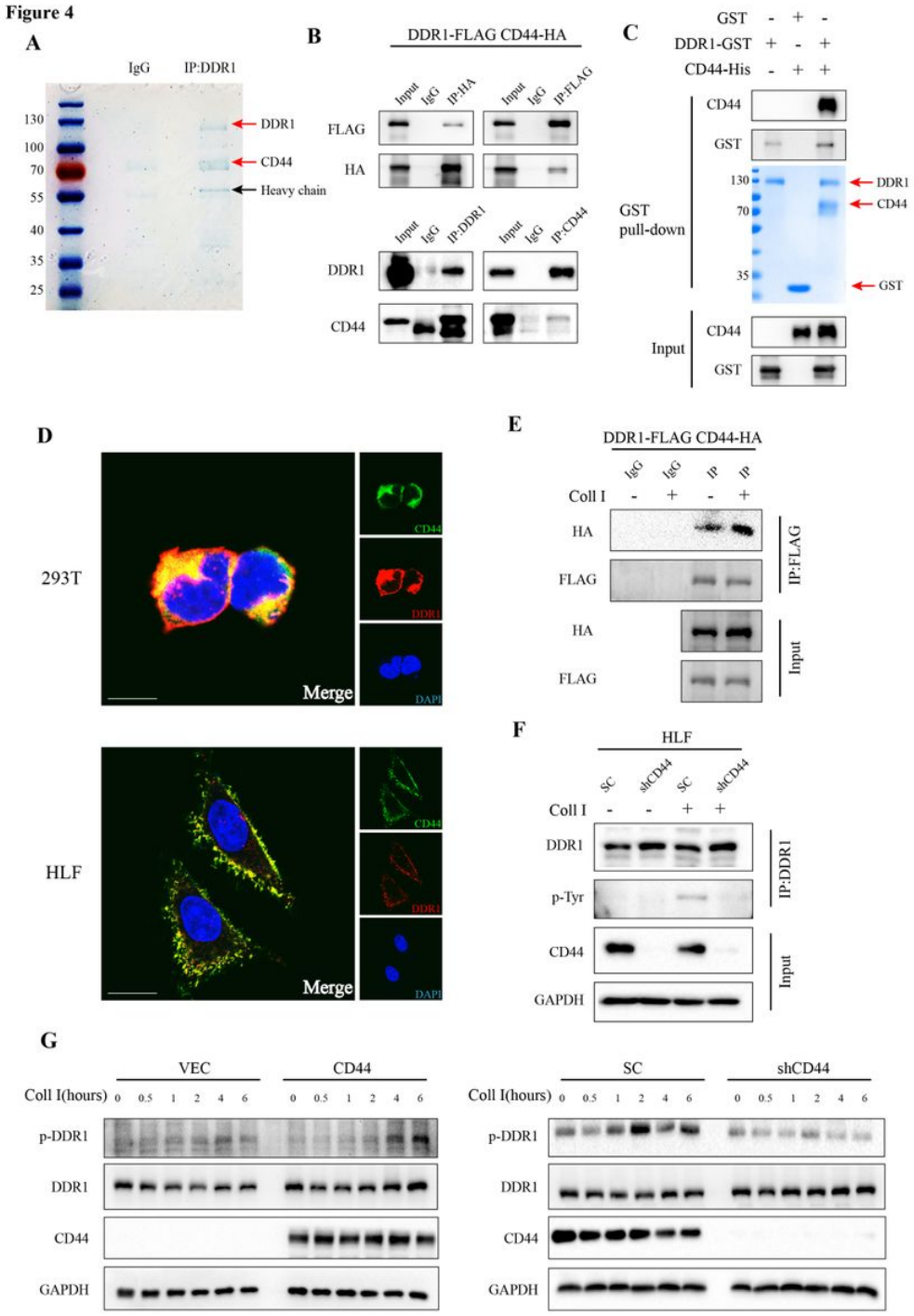


## Figure 4

### CD44 interacts with DDR1 and facilitates DDR1 phosphorylation.

(A) HLF cell lysates were immunoprecipitated with control rabbit IgG or anti-DDR1, ten percent of the cell extracts were loaded as an input, and immunoblotting and coomassie blue staining were performed.

(B) Co-immunoprecipitation (Co-IP) and immunoblotting assays for exogenously and endogenously expressed proteins were performed in HEK293T and HLF cells. Cross-validation by immunoprecipitation with anti-HA (or anti-CD44), immunoblotting with anti- FLAG (or anti-DDR1), immunoprecipitation with anti- FLAG (or anti-DDR1), and immunoblotting with anti-HA (or anti-CD44).

(C) GST pull-down assay showing direct interaction between DDR1 and CD44.

(D) Representative confocal images of immunofluorescence (IF) for CD44 (green), DDR1 (red), and nuclei (blue) in HEK293T and HLF cells (bar=10μm).

(E) DDR1- FLAG and CD44-HA were co-transfected into HEK293T cells and stimulated with or without collagen Ⅰ. Cells were lysed, and protein levels were analyzed by immunoblotting.

(F) HLF-shCD44 cells were stimulated with or without collagen Ⅰ, followed by immunoprecipitation with anti-DDR1 antibody and immunoblotting with anti- phosphorylated tyrosine.

(G) HLF-shCD44 and Hep3B-CD44 cells were stimulated with or without collagen Ⅰ for the indicated time periods. Phospho-DDR1 levels were measured using immunoblotting.

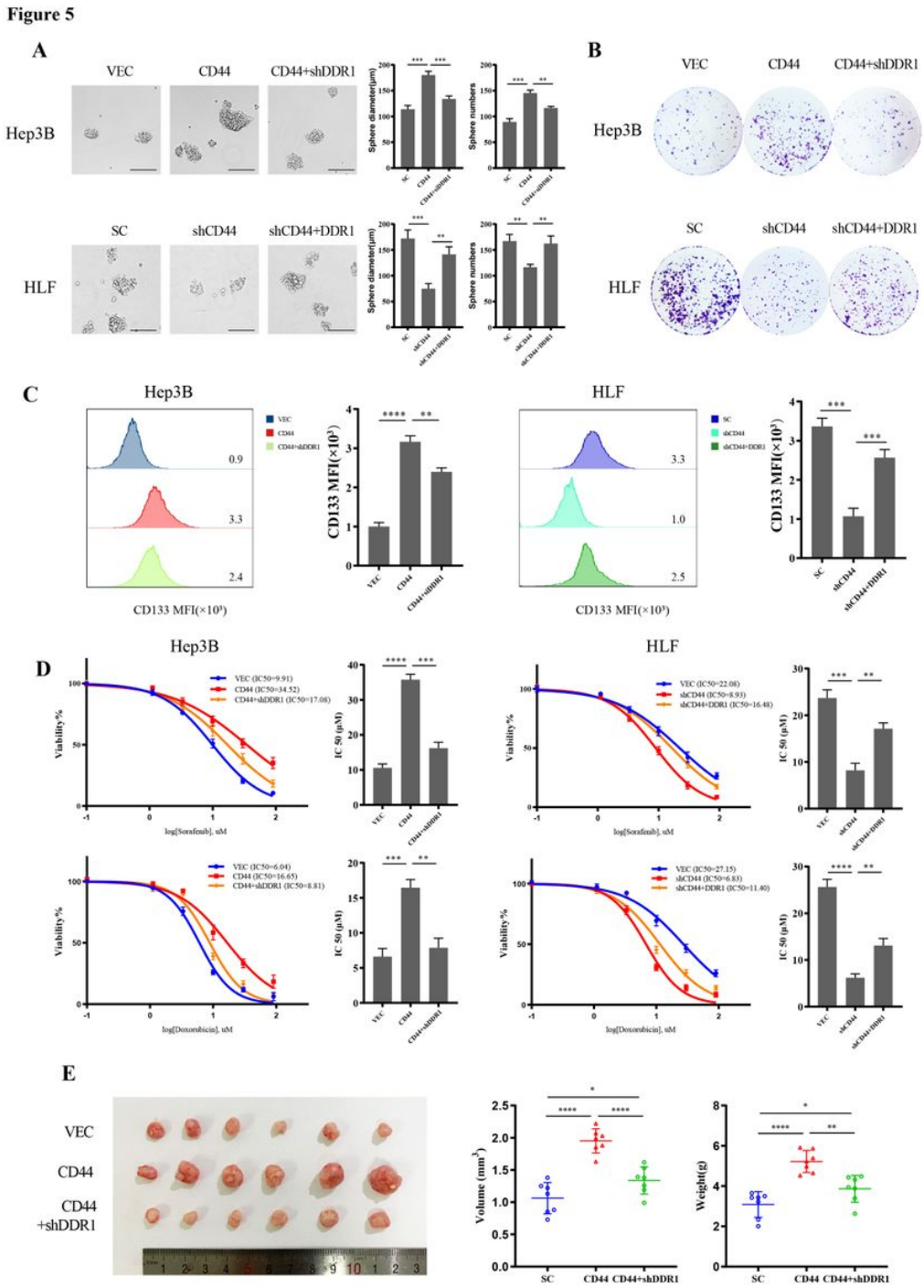


## Figure 5

**CD44 cross-talking with DDR1 enhances HCC cell lines' stemness *in vitro* and *vivo*.**

(A) Effects of CD44 knock-down with DDR1 overexpressed or overexpressed CD44 in the presence of DDR1 siRNA HCC cells on sphere-forming capacity, including sphere numbers and diameters (scale bar=200μm).

(B) Colony formation assay for CD44 knock-down with DDR1overexpressed or overexpressed CD44 in the presence of DDR1 siRNA HCC cells.

(C) Flow cytometry analyses of the CD133 mean fluorescence intensity in CD44 knock-down with DDR1overexpressed or overexpressed CD44 in the presence of DDR1 siRNA HCC cells. Error bars represent the standard deviation from three times independent experiments.

(D) Drug resistance to sorafenib or doxorubicin in CD44 knock-down with DDR1overexpressed or overexpress CD44 in the presence of DDR1 siRNA HCC cells. Cell viability was compared with the untreated cells, and IC50 values were calculated.

(E) 4 -week-old male nude mice were subcutaneously injected by a sphere-formed CD44 knock-down HCC cell line (n=6/group). Tumor weight and volume were shown in the right panel.

Two-tailed unpaired Student's t-test was performed. Each bar represents the mean ± SD.*$p < 0.05$, **$p < 0.01$, and ***$p < 0.001$

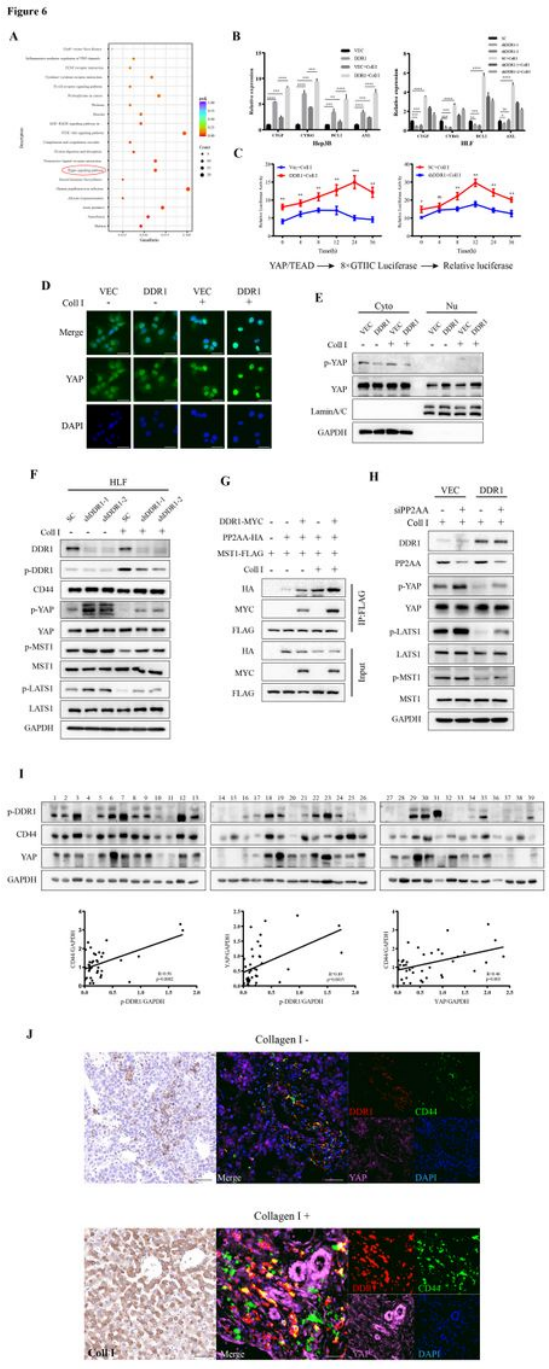

## Figure 6

### DDR1 impedes Hippo signaling through inactivating YAP.

(A) KEGG pathway analysis indicates that the Hippo signaling pathway was significantly affected by DDR1 knock-down HLF cells treated with collagen Ⅰ.

(B) mRNA expression levels of Hippo pathway downstream-associated genes in DDR1 knock-down or overexpress HCC cell lines.

(C) Luciferase reporter assays in DDR1 knock-down or overexpress HCC cells transfected with YAP/TAZ-responsive synthetic promoter-reporter plasmid and collagen Ⅰ treatment.

(D) Immunofluorescence assays display subcellular localization of YAP in DDR1 overexpress cell with collagen Ⅰ (scale bar=30μm).

(E) Nucleus/cytoplasm fractionation and immunoblotting analysis of DDR1 overexpress cells to show YAP nuclear translocation. GAPDH and Lamin A/C were used as cytoplasmic and nuclear markers, respectively.

(F) Effects of protein expression or phosphorylation of Hippo signaling components in DDR1 knock-down HLF cells.

(G) DDR1-Myc, PP2AA-HA, and MST1- FLAG were simultaneously transfected in HEK293T cells with or without collagen Ⅰ treatment, and evaluate the collagen Ⅰ contributed to the indicated protein interaction and stability by immunoblotting.

(H) DDR1 overexpress cells transfected with siPP2AA or control siRNA in the presence of collagen Ⅰ treatment. Immunoblotting analyzed the indicated protein from cell lysate. GAPDH is shown as the loading control.

(I) The protein level of phosphorylation DDR1, CD44, and YAP was measured in 39 HCC tissues by western blot. Representative western blot results were shown. GAPDH is shown as the loading control. Statistical analysis showed that p-DDR1, CD44, and YAP were pairwise positive upregulated in HCC tissues.

(J) Representative multiplex fluorescent immunohistochemical staining images of DDR1, CD44, and YAP in collagen Ⅰ poor or rich HCC sample, respectively (scale bar=100μm).

Two-tailed unpaired Student’s t test was performed. Each bar represents the mean ± SD.*$p < 0.05$, **$p < 0.01$, and ***$p < 0.001$

Figure 7

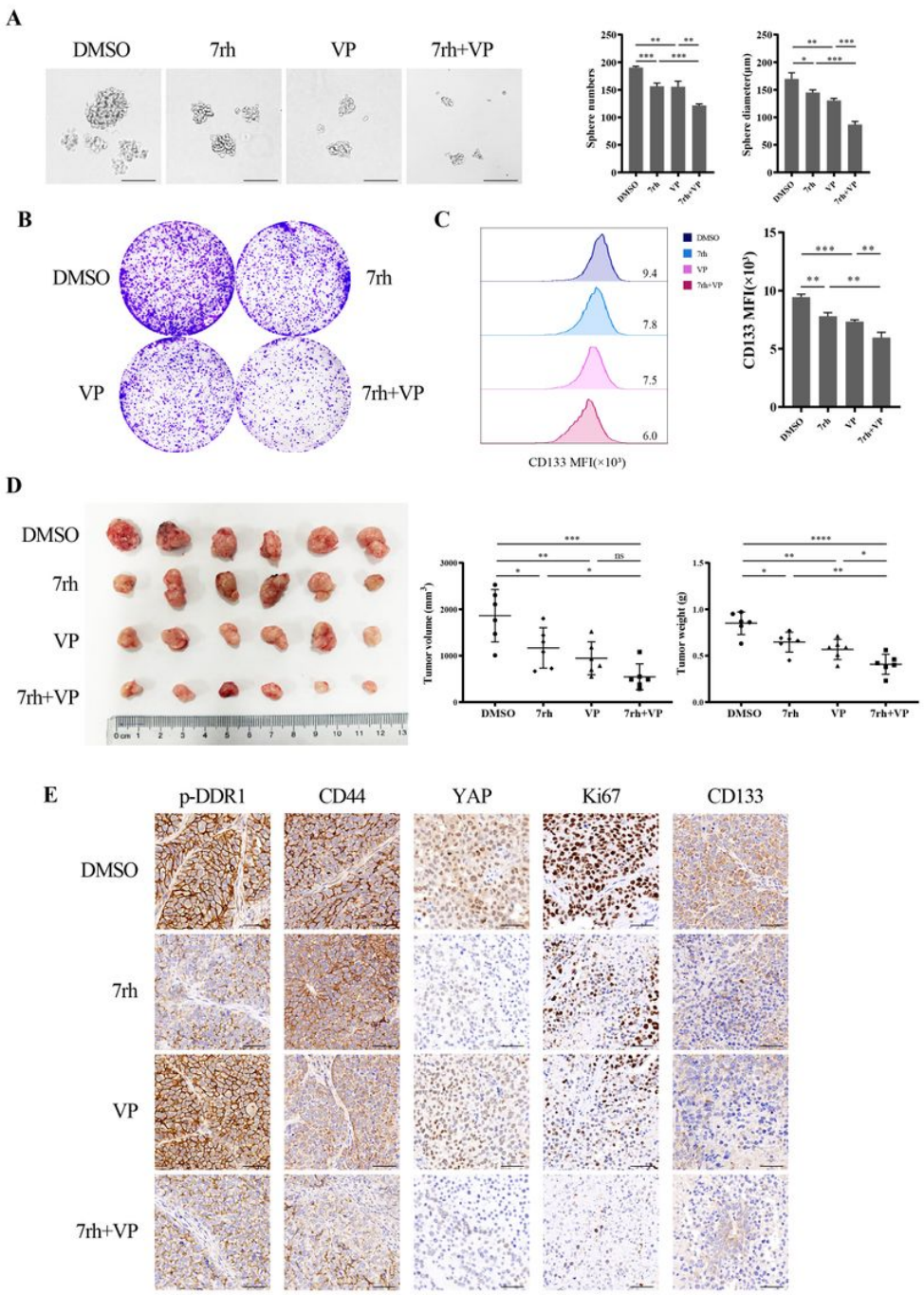


## Figure 7

**Co-inhibition of DDR1 and YAP signaling impedes tumor proliferation *in vitro and vivo*.**

(A) Effects of treatment with 7rh, VP, or combination therapy in HCC cell lines on sphere-forming capacity, sphere numbers, and diameters were counted. (scale bar=200μm).

(B) Colony formation assay of the 7rh, VP, or combination therapy treatment in HCC cell lines.

(C) Flow cytometry analyses of the CD133 mean fluorescence intensity in 7rh, VP, or combination therapy treatment in HCC cell lines. Error bars represent the standard deviation from three times independent

experiments.

(D) 4 -week-old male nude mice were subcutaneously injected by sphere-formed DDR1 overexpress HCC cell line, divided into DMSO, 7rh, VP, and combination groups randomly for 2 weeks of treatment (n=6/group). Tumor weight and volume were shown.

(E) Representative images of IHC staining of p-DDR1, CD44, Ki67, YAP, and CD133 (scale bar=100μm).

Two-tailed unpaired Student's t test was performed. Each bar represents the mean ± SD.*p < 0.05, **p < 0.01, and ***p < 0.001

**Figure 8**

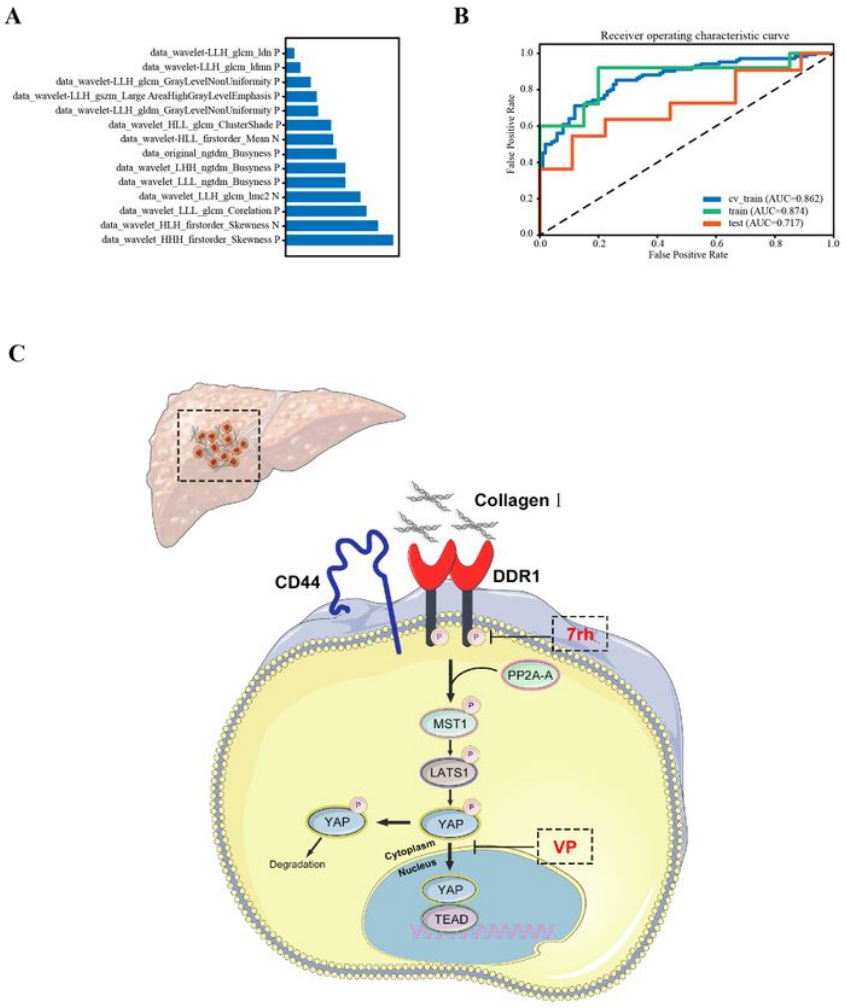

**Figure 8**

**Radiomics model of prediction on Collagen Ⅰ expression.**

(A) The important 14 features of the SVM classifier model in diagnosing HCC collagen Ⅰ expression.

(B) The ROC curves of models in train and test sets, respectively.

(C) The schematic diagram that collagen Ⅰ/DDR1 enhances HCC stemness through Hippo signaling.

# Supplementary Files

This is a list of supplementary files associated with this preprint. Click to download.

- SupplementaryTable1CorrelationbetweencollagenIExpressionwithClinicopathologicFeaturesinHCCn123.docx
- SupplementaryTable2.CorrelationbetweenDDR1ExpressionwithClinicopathologicFeaturesinHCCn123..docx
- SupplementaryTable3Genemicroarrayresults.docx
- SupplementaryTable4shRNAsiRNA.docx
- SupplementaryTable5primers.docx
- SupplementaryTable6antibody.docx
- SupplementaryTable7characteristics.docx
- supplmentary1.jpg
- supplmentary2.jpg
- supplmentary3.jpg
- supplmentary4.jpg